UCRL-ID-137718

A Preliminary Calculation of $^{235}U(n,2n)^{234}U$ Cross Sections

H. Chen, M.A. Ross, G. Reffo, R.M. White, W. Younes

November 23, 1999

U.S. Department of Energy
Lawrence Livermore National Laboratory

A Preliminary Calculation of ^{235}U(n,2n)^{234}U Cross Sections

H. Chen, M.A. Ross, G. Reffo, R.M. White, W. Younes

November 23, 1999

Lawrence Livermore National Laboratory

Abstract

Preliminary calculations of the total two-neutron emission cross section, ^{235}U(n,2n)^{234}U, and the partial two-neutron emission cross sections, ^{235}U$(n,2n\gamma)^{234}$U, are presented. The ^{235}U$(n,2n\gamma)^{234}$U cross sections describe the process of γ-decays in the residual nucleus following the two-neutron emission and were calculated for several γ-transitions between states of the ground-state band of the ^{234}U nucleus. All three reaction mechanisms, namely, direct, pre-equilibrium and compound, were included. In addition, fission competition as well as γ-cascade were considered in the compound component of the cross section calculations. A comparison with the relevant experimental data obtained from the GEANIE detector at the LANSCE/WNR facility in Los Alamos was also carried out.

1 Introduction

The ^{235}U(n,2n)^{234}U and ^{239}Pu(n,2n)^{238}Pu cross sections are of programmatic importance[1, 2, 3, 4, 5]. Because the direct measurements of these cross sections carry large uncertainties[6], a new experimental technique[3, 4, 5] which attempts to determine the cross sections indirectly is being conducted by the N-Division of Lawrence Livermore National Laboratory at the LANSCE/WNR facility of Los Alamos National Laboratory. In this technique, discrete γ-transitions between states of the ground-state band of the residual nuclei ^{234}U and ^{238}Pu are measured by the high-energy resolution γ-ray detector GEANIE. This establishes the partial ^{235}U$(n,2n\gamma)^{234}$U and ^{239}Pu$(n,2n\gamma)^{238}$Pu cross sections if absolute detector efficiencies are known. Theoretically calculated ratios of ^{235}U $(n,2n\gamma)^{234}$U/^{235}U$(n,2n)^{234}$U and
^{239}Pu$(n,2n\gamma)^{238}$Pu/^{239}Pu$(n,2n)^{238}$Pu are then used to derive the desired total ^{235}U$(n,2n)^{234}$U and ^{239}Pu$(n,2n)^{238}$Pu cross sections.

The ^{235}U and ^{239}Pu isotopes have similar nuclear properties. An example is the Q-value of the (n,2n) reaction in both cases. However, in the energy range of 5 to 20 MeV of incident neutrons, the fission cross section of ^{235}U, on average, is about 30% lower than that of ^{239}Pu. At the (n,2n) threshold, the cross section of the ^{239}Pu(n,f) reaction is about 58% higher than that of ^{235}U(n,f). The reduced fission background in the n+^{235}U reaction results in smaller statistical errors in the new indirect measurements. Also in favor of the ^{235}U as a target is its much reduced radioactivity. Direct comparisons between the experimentally measured and the theoretically calculated $^{235}\mathrm{U}(n,2n\gamma)^{234}\mathrm{U}$ partial cross sections thus have increased reliability. Furthermore, the reduced background of fission neutrons in the n+^{235}U reaction establishes the ^{235}U(n,2n)^{234}U cross section measurement by direct neutron counting technique with less uncertainty than its ^{239}Pu(n,2n)^{238}Pu counterpart measurement. Since the derivation of the total ^{235}U(n,2n)^{234}U cross section from the new indirect measurements is based on the theoretically calculated ratios of $(n,2n\gamma)/(n,2n)$, a comparison of the total ^{235}U(n,2n)^{234}U cross section between the direct neutron counting measurement and that derived from the indirect γ-ray measurement provides a measure of the accuracy of the new technique as well as the theoretical calculation of the ratios of $(n,2n\gamma)/(n,2n)$.

This report presents preliminary theoretical calculations of the $^{235}\mathrm{U}(n,2n\gamma)^{234}\mathrm{U}/^{235}\mathrm{U}(n,2n)^{234}\mathrm{U}$ ratios and relevant cross sections. Experiments were ongoing at the time of these calculations. Hence, the comparison with the experimental data in this report is based on available preliminary experimental information.

2 Results and Discussions

The three major reaction mechanisms adopted are the direct, the preequilibrium, and the compound reactions. Cross sections of direct reaction channels are given by the optical model which approximates the nuclear interactions by a nucleon-nucleus potential[7]. Preequilibrium treatment for neutron emissions is based on the exciton model[8, 9, 10, 11, 12, 13, 14] whereas compound emissions are calculated using the Hauser-Feshbach formalism[15]. Gamma decays are considered as a compound process and they are computed using the Brink-Axel approach[16, 17]. Additionally, the fission process is considered as a competing channel for the equilibrium decays. Fission transmission coefficients are calculated from the double-humped fission barrier model of Bjornholm and Lynn[18]. The physics models employed for the n+^{235}U and n+^{239}Pu reactions are identical[1]. The calculations were carried out with the IDA[20] system of codes.

To study the behavior of the $^{235}\mathrm{U}(n,2n)^{234}\mathrm{U}$ cross section, we focused on the

[1]For more detailed explanations of the models, readers are referred to References 1 and 2, as well as in the quoted references above.

energy range of incident neutrons from 5.5 MeV to 17.5 MeV. The $^{235}\mathrm{U}(n,2n)$, $^{235}\mathrm{U}(n,3n)$ and $^{235}\mathrm{U}(n,4n)$ thresholds are, respectively, 5.298 MeV, 12.141 MeV and 17.895 MeV. Since the $^{235}\mathrm{U}(n,2n)$ cross section becomes small before the $^{235}\mathrm{U}(n,4n)$ reaction channel opens up, our calculations were carried out up to 17.5 MeV.

2.1 Total Cross Section

The total cross section, σ_{t}, reaction cross section, σ_{R}, and the shape elastic cross section $\sigma_{\mathrm{s.e}}$ are related by

$$\sigma_{\mathrm{t}} = \sigma_{\mathrm{R}} + \sigma_{\mathrm{s.e}}\,. \tag{1}$$

These cross sections were calculated using the optical model codes ECIS[19] and CIRCE[20]. When the same input parameters were used, the two codes returned identical results. Because the $^{235}\mathrm{U}$ nucleus is deformed, the coupled channel option in the codes was utilized[21]. Specifically, the first three states in the ground state band of $^{235}\mathrm{U}$ were coupled. The excitation energy, spin and parity of these states are: (0 keV, 7/2, −), (46.204 keV, 9/2, −) and (103.032 keV, 11/2, −), respectively. Optical model parameters of Dietrich[22] and Madland[23] were considered. As can be seen from Figure 1, both potentials give good agreement with the evaluated experimental data. The Madland's optical model parameters were used for the entire range of neutron incident energy from 5.5 to 17.5 MeV, although they were designed for incident neutron energies of under 10 MeV. The evaluated total cross section is the latest result from White[26] and represents a conclusion drawn from 25 sets of experimental data. The estimated uncertainty of the evaluation is no more than 1%. For the purpose of comparison, the ENDF/B-VI evaluation[29] is also plotted in the figure. Overall, the agreement between the calculated total cross section, using Dietrich's potential, with the evaluated experimental data is less than 3%.

2.2 Reaction Cross Section

The magnitude of the reaction cross section, σ_{R}, is of critical importance. It provides an overall scaling of cross sections for all subsequent reaction channels. Out of the reaction channels that sum up to the reaction cross section, the particle-emission cross sections are further divided into contributions from the preequilibrium and the equilibrium reaction mechanisms. An additional direct component in the (n,n') reaction channel is present when the coupled-channel option in the optical model is used. Clearly, an accurate calculation of σ_{R} is the first step towards correctly predicting the cross sections of all reaction channels that follow the formation of the composite nucleus.

In our calculations, preequilibrium γ-emissions were not considered. Also neglected were proton and other charged-particle emissions which are significantly attenuated due to the presence of Coulomb barriers. Furthermore, when the incident neutron energy is greater than 2 MeV, the compound elastic scattering cross section, $\sigma_{\rm comp}(n,n)$, becomes negligibly small. In the energy range of our interest, the capture cross section, $\sigma(n,\gamma)$, is also negligible. We can therefore ignore these two components and we thus have,

$$\sigma_{\rm R} = \sigma(n,f) + \sigma(n,n') + \sigma(n,2n) + \sigma(n,3n)\,. \tag{2}$$

When $\sigma_{\rm comp}(n,n)$ is ignored, $\sigma_{\rm R}$ becomes identical to $\sigma(n,{\rm nonelastic})$ where

$$\sigma_{\rm t} = \sigma(n,{\rm elastic}) + \sigma(n,{\rm nonelastic})\,. \tag{3}$$

Figure 2 shows two calculations of $\sigma(n,{\rm nonelastic})$ together with the experimental data that could be found from the EXFOR[30] data base. Where $\sigma_{\rm comp}(n,n)$ was non-zero, it was subtracted from the calculated $\sigma_{\rm R}$ to obtain $\sigma(n,{\rm nonelastic})$.

As can be seen, variations between different sets of experimental data are large. The difference between the two calculated curves is purely a result of the two different sets of optical model parameters employed. Dietrich's parameters give rise to a reaction cross section that is approximately 7% higher than that obtained from Madland's parameters. Since experimental data on $\sigma(n,{\rm nonelastic})$ cannot differentiate one set of optical model parameters from another, we chose Dietrich's parameters for the $(n,2n)$ cross section calculations because of the closer agreement with the experimentally-measured total cross sections. We note, however, that the Madland's parameters we used are not his latest set which is known to generate total cross sections that are in better agreement with experimental data[24, 22].

Accuracy of the calculated $\sigma_{\rm R}$ can be examined against experimental data on angular distribution of elastic scattering cross sections, provided the $\sigma_{\rm comp}(n,n)$ cross section is negligible. Unfortunately, as is the case with $\sigma_{\rm R}$, experimental data of such angular distributions are scarce. Figures 3 and 4 give comparisons between the theoretical calculations and the experimental data at $E_{\rm inc} = 5$ MeV and $E_{\rm inc} = 5.5$ MeV. It is seen that Dietrich's parameters give good agreement with the data at these incident neutron energies. Note, however, that these incident energies are just below and above the ^{235}U(n,2n) threshold and are not sufficient to support the energy dependence of the reaction cross section.

2.3 Fission Cross Section

For the ^{235}U nucleus, the neutron-induced fission cross section, $\sigma(n,f)$, is a large component of the reaction cross section, $\sigma_{\rm R}$, as can be seen from Figure 5. Values of the fission barrier heights and curvatures at the saddle points for the involved fissioning isotopes ^{236}U, ^{235}U, and ^{234}U were taken from the review article by

Bjornholm and Lynn[18]. The fission transmission coefficient, $T(J,\pi,E)$, through a single potential barrier whose shape is approximated by an inverted parabola is given by Hill and Wheeler[25] as

$$T(J,\pi,E) = \int_0^\infty \frac{\rho(J,\pi,\epsilon)d\epsilon}{1+\exp\left[V+\epsilon-E\right]/\hbar\omega}. \tag{4}$$

In equation (4), E is the excitation energy of the given nucleus measured from the ground state, J is the total angular momentum of the nucleus, V is the fission barrier height and $\hbar\omega$ is the curvature of the barrier at the saddle point. The two barriers in the double-humped fission model were assumed to be uncorrelated and the total transmission coefficient through both barriers A and B is simply

$$T(J,\pi,E) = \frac{T_A(J,\pi,E)T_B(J,\pi,E)}{T_A(J,\pi,E)+T_B(J,\pi,E)}. \tag{5}$$

Both V and $\hbar\omega$ were assumed to be independent of J,π and E. The dependence of the fission transmission coefficients on J comes solely from the level density $\rho(J,E,\pi)$, and $\rho(J,\pi=+,E)=\rho(J,\pi=-,E)$ was assumed. The energy dependence of the level density above the saddle point was taken to be of the constant temperature type such that

$$\tilde{\rho}(J,E) = \rho_J(J)\rho(E) = \frac{(2J+1)\exp\left[-(J+1/2)^2/2\sigma^2\right]}{2\sqrt{2\pi}\sigma^2}\rho(E) \tag{6}$$

$$\rho(E) = \sum_J \tilde{\rho}(J,E) = C\exp E/\theta \tag{7}$$

where C is a constant and θ is the nuclear temperature. The spin-cutoff parameter σ^2 was assumed to be a constant. It was suggested by Bjornholm and Lynn that different parameters C and θ be used for different ranges of the excitation energy. These suggested parameters[18] were employed in our calculations.

Again, the difference between the two sets of calculations in Figure 5 is entirely due to the differences in the optical model parameters. The increase in fission cross section due to the second-chance fission is clearly seen in both calculations while that due to the third-chance fission is better reproduced in the calculation based on Dietrich's optical model parameters. Recall that Dietrich's parameters lead to a σ_R that is higher than that obtained with Madland's parameters over the energy range of our concern. One sees from Figure 5 that the former leads to an overestimate of the fission cross section while an underestimate was produced by the latter. This demonstrates the importance of a correct calculation of σ_R. On average, the overestimation of the calculated fission cross section is about 15% as is the underestimation. The ENDL99 evaluation of the fission cross section is the newest analysis of 60 sets of experimental data[26] and the uncertainty of this evaluation is less than 1.5%.

2.4 Inelastic Scattering Cross Section

Another reaction channel to be considered in order to examine the $(n, 2n)$ cross section is the inelastic scattering cross section $^{235}\mathrm{U}(n, n')$. All the calculations from here on are based on the optical model parameters from Dietrich. Figure 6 shows the calculated $^{235}\mathrm{U}(n, n')$ cross sections. For the purpose of comparison, the ENDL [27] and ENDF/B-VI evaluations are also shown in the figure. The rapid decrease in the cross section between 5 and 7 MeV incident neutron energy is due to the opening up of the $(n, 2n)$ channel. There are three components to the $^{235}\mathrm{U}(n, n')$ cross section. Namely, the direct, preequilibrium and compound components. Figure 7 displays the ratios of each of these components to the total $^{235}\mathrm{U}(n, n')$ cross section. It is seen that the compound component decreases quickly as the incident neutron energy increases around the threshold of the $(n, 2n)$ cross section. This is simply a consequence of the competition between the (n, n') and $(n, 2n)$ reactions in the compound decay process. The preequilibrium emission is favored when the incident neutron energy is high, hence the general upward trend with the increase of E_{inc}. The direct component is calculated from the optical model by the code ECIS. It follows the behavior of the total cross section which is fairly flat over this energy range. When $E_{\mathrm{inc}} < 6$ MeV, the (n, n') channel is clearly dominated by the compound process and both the preequilibrium and the direct components of the (n, n') cross section are low in percentage. All calculations were carried out in 1 MeV incident neutron energy steps except the first and the last points which were calculated at 5.5 MeV and 17.5 MeV. This energy binning gives rise to some unsmoothness in the curves.

2.5 The $^{235}\mathrm{U}(n, 2n\gamma)^{234}\mathrm{U}$ And $^{235}\mathrm{U}(n, 2n)^{234}\mathrm{U}$ Cross Sections

Partial $^{235}\mathrm{U}(n, 2n\gamma)^{234}\mathrm{U}$ cross sections for various γ-transitions in the $^{234}\mathrm{U}$ nucleus were calculated. Specifically, the probability of populating the 10_1^+, 8_1^+, 6_1^+, 4_1^+, and 2_1^+ states of the ground state band were computed. The excitation energies of these states are 741.2 keV, 497.0 keV, 296.1 keV, 143.4 keV, and 43.5 keV, respectively. When available, experimental branching ratios for γ-transitions between discrete states were used. The branching ratios that are not identified experimentally are supplemented by model calculations. The $2_1^+ \rightarrow 0_1^+$ γ-ray, having an energy of 43.5 keV, cannot be measured due to target attenuation and internal conversion. Plotted in Figures 8 to 11 are the IDA calculations of the aforementioned partial cross sections together with the experimental data obtained from the GEANIE detector[5]. The experimental data provided the shapes of the partial cross sections and they were normalized, by a multiplicative factor, to the theory curves from IDA calculations. Also shown in these figures are calculations from GNASH[28] by Chadwick. It is seen that the experimental data normalized to IDA calculations agree well in shape in all four excitation functions, especially for the $4_1^+ \rightarrow 2_1^+$ transition. Better statistics for the measured intensities of the

$6_1^+ \rightarrow 4_1^+$ and $8_1^+ \rightarrow 6_1^+$ transitions lead to smaller experimental error bars. For given excitation functions of the reaction and fission cross sections, the shapes and absolute values of the $^{235}\mathrm{U}(n, 2n\gamma)$ excitation functions are a result of the interplay between the preequilibrium and the compound processes as well as various particle-emission channels. At the $(n, 2n)$ threshold, the competition between one- and two-neutron emissions is particularly important in addition to the competition between the preequilibrium and the compound processes. Similarly, the competition between the $(n, 2n)$ and $(n, 3n)$ emissions and between the preequilibrium and the equilibrium processes affects the behavior of the tails of the excitation functions. Additionally, the γ-cascade mechanism would also influence the $^{235}\mathrm{U}(n, 2n\gamma)$ excitation functions both in shape and absolute values.

Examination of the IDA calculations from figures 8 to 11 shows that the peaks of the excitation functions do not shift much with the change of angular momentum. This feature is also seen in the experimental data. From Figures 8 to 11, one notices that the GNASH calculations predict higher partial cross sections than the IDA calculations, especially at high excitation energies. This is probably due to the differences in the calculation of the preequilibrium emissions. Also noticed is the increasing difference between IDA and GNASH calculations as the spin of the populated state goes up. This suggests that different spin distributions of the residual nucleus are employed in the two codes. Of course, the difference in calculated reaction cross sections, to begin with, could contribute to the differences in the calculated partial cross sections from IDA and GNASH. Another possible source of discrepancy could be the calculated fission cross sections. Further investigation of the reasons for the differences between the two calculations should be carried out.

The calculated ratios of the partial $(n, 2n\gamma)$ cross sections to the total $(n, 2n)$ cross section are shown in Figure 12. Since the branching ratios for the $10_1^+ \rightarrow 8_1^+$, $8_1^+ \rightarrow 6_1^+$, $6_1^+ \rightarrow 4_1^+$, and $4_1^+ \rightarrow 2_1^+$ transitions within the ground state band are all 100%, the population of the state 10_1^+ ensures the population of states of lower spins. However, the converse is not true. One therefore sees that the ratio of $^{235}\mathrm{U}(n, 2n\gamma^{4_1^+ \rightarrow 2_1^+})/^{234}\mathrm{U}(n, 2n)$ is higher than that of $^{235}\mathrm{U}(n, 2n\gamma^{6_1^+ \rightarrow 4_1^+})/^{234}\mathrm{U}(n, 2n)$, for example. The shift of thresholds of these ratios is simply a result of energetics. Figure 12 also shows that as E_{inc} increases, the ratios associated with various transitions become relatively flat.

Figure 13 shows the total $^{235}\mathrm{U}(n, 2n)^{234}\mathrm{U}$ cross sections calculated from IDA and GNASH as well as data from direct measurements by Frehaut[6] and Mather. One sees that the calculated threshold behavior agrees fairly well with the Frehaut measurements. However, the IDA calculations of the $^{235}\mathrm{U}(n, 2n)^{234}\mathrm{U}$ cross sections yielded lower values than those measured by Frehaut and Mather between 7 and 13 MeV of incident neutron energy whereas the calculated value is higher at $E_{\mathrm{inc}} = 14$ MeV. The GNASH calculations are consistently higher than those from IDA. Given the uncertainties in both the experimental measurements and

the theoretical calculations, the discrepancies between IDA and GNASH and the data are not surprising. The large experimental uncertainties are mostly due to the contamination of fission neutrons in the direct measurement of the ^{235}U$(n, 2n)$ cross section[5]. The theoretical uncertainties can come from several sources which are discussed in Section2.7. For fixed reaction and fission cross sections, the calculated $(n, 2n)$ cross section at various incident neutron energies sensitively depends on the magnitude of the preequilibrium neutron emission cross section. Despite the existing discrepancies, the overall agreement between theory and measurements by Frehaut and Mather is good.

2.6 Sensitivity Of Calculations On Discrete Spectroscopy

The spectroscopy of the discrete, low-lying states of ^{234}U directly affects the calculation of γ-cascade through these levels. It is therefore of interest to investigate the effects of the discrete spectroscopy on the calculated $(n, 2n\gamma)$ cross sections and the derived ratios of $(n, 2n\gamma)/(n, 2n)$.

In the low excitation energy region where excited states of a given nucleus are discrete, experimental data[31] on the levels, when available, are used for cross section calculations. These data include the excitation energy, the spin and the parity of the excited states. Continuous level density formulae take over when such experimental information becomes ambiguous. The excitation energy at which this switch-over occurs is denoted by $E_{\rm cut}$. For the ^{234}U nucleus, $E_{\rm cut} = 1.14$ MeV was used in our calculations because the spin and parity of some states beyond this energy are not positively identified experimentally. In order to see if extended experimental information on the discrete spectroscopy would make a difference on the modeling of various reaction cross sections, calculations were repeated with $E_{\rm cut}$ reduced to 0.57 MeV. Figures 14 to 16 show the results of the calculated ^{235}U$(n, 2n\gamma^{6_1^+\to 4_1^+})$, ^{235}U$(n, 2n\gamma^{6_1^+\to 4_1^+})/^{235}U(n, 2n)$ and the percentage change of this ratio due to the reduction of $E_{\rm cut}$.

One sees from Figure 14 that the difference made to the partial cross section $(n, 2n\gamma)$ ranges from 7% to 21% with the largest impact shown near 7 MeV incident neutron energy. On the other hand, the reduction of $E_{\rm cut}$ had no effect on the total $(n, 2n)$ cross section as expected. This, of course, leads to a sizable difference on the ratio of $(n, 2n\gamma^{6_1^+\to 4_1^+})/(n, 2n)$ shown in Figure 15. The solid line in Figure 15 is the ratio calculated at $E_{\rm cut} = 1.14$ MeV for the ^{234}U nucleus whereas the dashed line is the same ratio calculated at $E_{\rm cut} = 0.57$ MeV. It is seen from Figure 15 that the difference between the two curves is as large as 14% around 13 MeV incident neutron energy. Since the indirect measurement of the total $(n, 2n)$ cross section depends on the theoretically calculated ratio of $(n, 2n\gamma)/(n, 2n)$, it is evident that the best spectroscopy information is required in order to minimize the uncertainty in the calculation of this ratio. To see the percentage variation of the ratio due to the decrease of $E_{\rm cut}$, we computed the quantity Δratio/ratio where

$$\frac{\Delta\text{ratio}}{\text{ratio}} = \frac{\text{ratio}(E_{\text{cut}} = 1.14) - \text{ratio}(E_{\text{cut}} = 0.57)}{\text{ratio}(E_{\text{cut}} = 1.14)} \tag{8}$$

$$\text{ratio} = \frac{^{235}\text{U}(n, 2n\gamma)}{^{235}\text{U}(n, 2n)}. \tag{9}$$

Figure 16 shows the calculations of Equation (8) for the $4_1^+ \rightarrow 2_1^+$ and $6_1^+ \rightarrow 4_1^+$ γ-transitions. As one would expect, the effect of decreasing E_{cut} is larger on the $6_1^+ \rightarrow 4_1^+$ γ-transition than the $4_1^+ \rightarrow 2_1^+$ γ-transition.

2.7 Uncertainties Of Calculations

Given an optical model potential, the magnitude of the reaction cross section is determined by the parameters of the potential. Unfortunately, the lack of experimental data on the reaction cross section does not allow a unique determination of these parameters. Consequently, it is difficult to quantify the uncertainties associated with the reaction cross section. This uncertainty constitutes the primary source of error in our calculated absolute cross sections. To facilitate the determination of the magnitude of the reaction cross section σ_{R}, additional experimental data on the angular distribution of the elastic scattering channel would be useful.

The second source of uncertainty comes from the calculation of fission cross sections. It is seen that the fission cross section is a large component of the reaction cross section. Uncertainties in this cross section could therefore have significant impact on the desired $(n, 2n)$ cross section. A proper description of the complex fission process is extremely difficult, although improved fission models would be of help. When the fission model is giving correct physical trend, we could take advantage of the well-established experimental fission cross sections and adjust the parameters in the fission model to correct the magnitude of fission cross sections. This would exclude fission as a source of uncertainty from calculations.

The third component of uncertainty comes from the treatment of preequilibrium particle emissions. Different models which describe this process lead to results that differ from each other significantly. Adding to an already complicated process is the fact that particles emitted via the preequilibrium mechanism carry with them, on average, more angular momentum than the evaporated particles. This results in a smaller angular momentum transfer to the residual nucleus as well as a different angular momentum distribution in the residual nucleus. A proper treatment of both is important for the calculation of the population of a state with a given spin. This in turn affects the calculation of the ratio of $(n, 2n\gamma)/(n, 2n)$. Clearly, more research is needed on this subject.

Finally, level densities remain as a significant source of uncertainty, especially for the calculation of absolute cross sections. This applies to level density formulations used in the compound process, the preequilibrium process or the fission

process. In calculating the ratios, because the uncertainties appear both in the numerator and the denominator, they cancel to a certain extent. However, some uncertainties particularly affect the partial cross sections, and therefore the ratios. An example of this, given in the previous section, is the effect of discrete spectroscopy. The description of γ-cascade is also especially relevant to the ratios. Another potential uncertainty in the calculated ratios of $(n, 2n\gamma)/(n, 2n)$ is associated with the angular momentum transfer to and its distribution in the residual nucleus following preequilibrium particle emissions.

3 Conclusions

To derive the total $^{235}\mathrm{U}(n, 2n)^{234}\mathrm{U}$ cross section from the indirect experimental measurement carried out by N-Division, the ratio of $^{235}\mathrm{U}(n, 2n\gamma)^{234}\mathrm{U}/^{235}\mathrm{U}(n, 2n)^{234}\mathrm{U}$ must be calculated. To obtain a reliable prediction of this ratio, accurate calculations of cross sections of all involved channels are necessary. Results of a preliminary calculation are summarized in this report. It is shown that the calculated partial $^{235}\mathrm{U}(n, 2n\gamma)^{234}\mathrm{U}$ cross sections agree well in shape with the preliminary experimental data obtained from the GEANIE detector. Good agreement between the calculated total $^{235}\mathrm{U}(n, 2n)^{234}\mathrm{U}$ cross section and those measured by Frehaut and Mather was also achieved.

In conclusion, our preliminary calculations are encouraging. Further improvements and discussions of the differences between the IDA and the GNASH calculations are planned to reduce the theoretical uncertainties.

4 Acknowledgements

Discussions with Lee Bernstein, Marshall Blann and Frank Dietrich on the calculations presented in this report are greatfully acknowledged. The authors wish to thank Mark Chadwick for providing GNASH calculations.

References

[1] M.A. Ross, H. Chen, G. Reffo and R.M. White, "The $^{239}\mathrm{Pu}(n, 2n)^{238}\mathrm{Pu}$ Cross Section: Preliminary Calculations", UCRL-ID-**133497**, Lawrence Livermore National Laboratory, (1999).

[2] M. Chadwick, "Calculated Plutonium Reactions for Determining $^{239}\mathrm{Pu}(n, 2n)^{238}\mathrm{Pu}$", report, Los Alamos National Laboratory, (1999).

[3] J.A. Becker and M.B. Chadwick, "Measurement of the $^{239}\mathrm{Pu}(n, 2n)$ Cross Section Between Threshold and 15 MeV", (1995), private communication.

[4] L.A. Bernstein, "^{239}Pu$(n,2n)^{238}$Pu Measurement Proposal", (1997), private communication.

[5] W. Younes, J.A. Becker, L.A Bernstein, D.E. Archer, M.A. Stoyer, D.P. McNabb, K. Hauschild, D.M. Drake, G.D. Johns, R.O. Nelson, and W.S. Wilburn, "Measurement of the ^{235}U$(n,2n)$ Cross Section using GEANIE at LANSCE/WNR: Progress Report on the 1997 Data and Analysis Techniques", UCRL-ID-**132627**, Lawrence Livermore National Laboratory, (1998).

[6] J. Frehaut, A. Bertin, and R. Bois, "Measurement of the ^{235}U$(n,2n)$ Cross Section Between Threshold and 13 MeV", *Nucl. Sci. Eng.*, **74**, 29(1980).

[7] P.E. Hodgson, "The Optical Model of Elastic Scattering", Oxford University Press, (1963).

[8] J.M. Akkermans, H. Gruppelaar, and G. Reffo, *Phys. Rev. C* **22**, 73(1980).

[9] J.J. Griffin, *Phys. Rev. Lett.* **17**, 478(1966).

[10] D. Agassi, H.A. Weidenmuller and G. Mantzouranis, *Phys. Rep.* **22C**, 147(1975).

[11] H. Nishioka, J.J.M. Verbaarschot, H.A. Weidenmuller and S. Yoshida, *Ann. Phys.* (N.Y.). **172**, 67(1986).

[12] H. Nishioka, H.A. Weidenmuller and S. Yoshida, *Ann. Phys.* (N.Y.). **183**, 166(1988).

[13] G. Reffo, C. Costa, and F. Fabbri, ENEA report RT/FI(83)10.

[14] G. Reffo and C. Costa, "International Conference on Nuclear Physics", Florence, August 29 to September 3, 1983. Edited by A. Ricci, Published by Tipografia Compositori, Bologna, **Vol. 1**, 85(1983).

[15] W. Hauser and H. Feshbach, *Phys. Rev.* **87**, 366(1952).

[16] D.M. Brink, *D. Phil. Thesis*, University of Oxford, (1955).

[17] P. Axel, *Phys. Rev.*, **126**, 671(1962).

[18] S.E. Bjornholm and J.E. Lynn, "The Double-Humped Fission Barrier", *Rev. Mod. Phys.*, **52**, 725(1980).

[19] J. Raynal, code ECIS95, unpublished.

[20] G. Reffo and F. Fabbri, IDA system of codes, ENEA, Bologna, Italy.

[21] G.R. Satchler, "Introduction to Nuclear Reactions", Second Edition, Oxford University Press, (1990).

[22] F. Dietrich, private communication.

[23] D.G. Madland and P.G. Young, "Neutron-Nucleus Optical Potential for the Actinides Region", International Conference on Neutron Physics and Neutron Data for Reactors and Other Applied Purpose, September 25-29, 1978, United Kingdom.

[24] P. Young, "Experience at Los Alamos With Use of the Optical Model for Applied Nuclear Data Calculations". INDC(NDS)-335, page 109, International Atomic Energy Agency, compiled by P. Oblozinsky, 1995.

[25] D.L. Hill and J.A. Wheeler, *Rev. Mod. Phys.*, **89**, 1102(1953).

[26] R.M. White, ENDL99, private communication.

[27] R.J.Howerton and R.M White, private communication.

[28] M.B. Chadwick, Los Alamos National Laboratory, Memorandum **T-2-98-49**, August 21, (1998).

[29] P. Rose, "ENDF-201: ENDF/B Summary Documentation", Fourth Edition (ENDF/B-VI), Brookhaven National Laboratory report, BNL-NCS-**17541**, (1992).

[30] V. McLane, "EXFOR Basics - A Short Guide to the Nuclear Reaction Data Exchange Format", BNL-NCS-**63380**, Brookhaven National Laboratory, 1996.

[31] Evaluated Nuclear Structure Data File, maintained by Brookhaven National Laboratory.

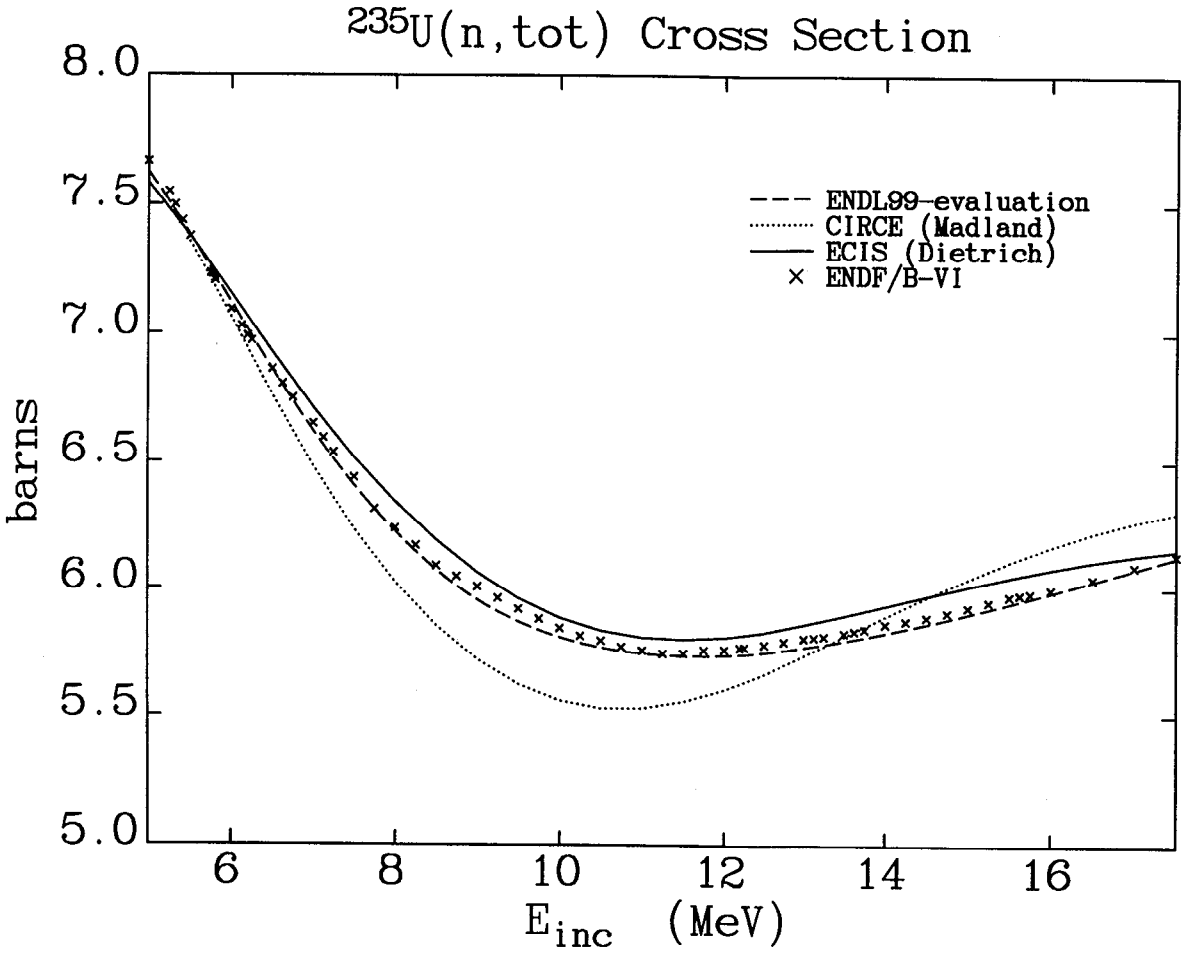

Figure 1: *n+^{235}U total cross section as a function of incident neutron energy.*

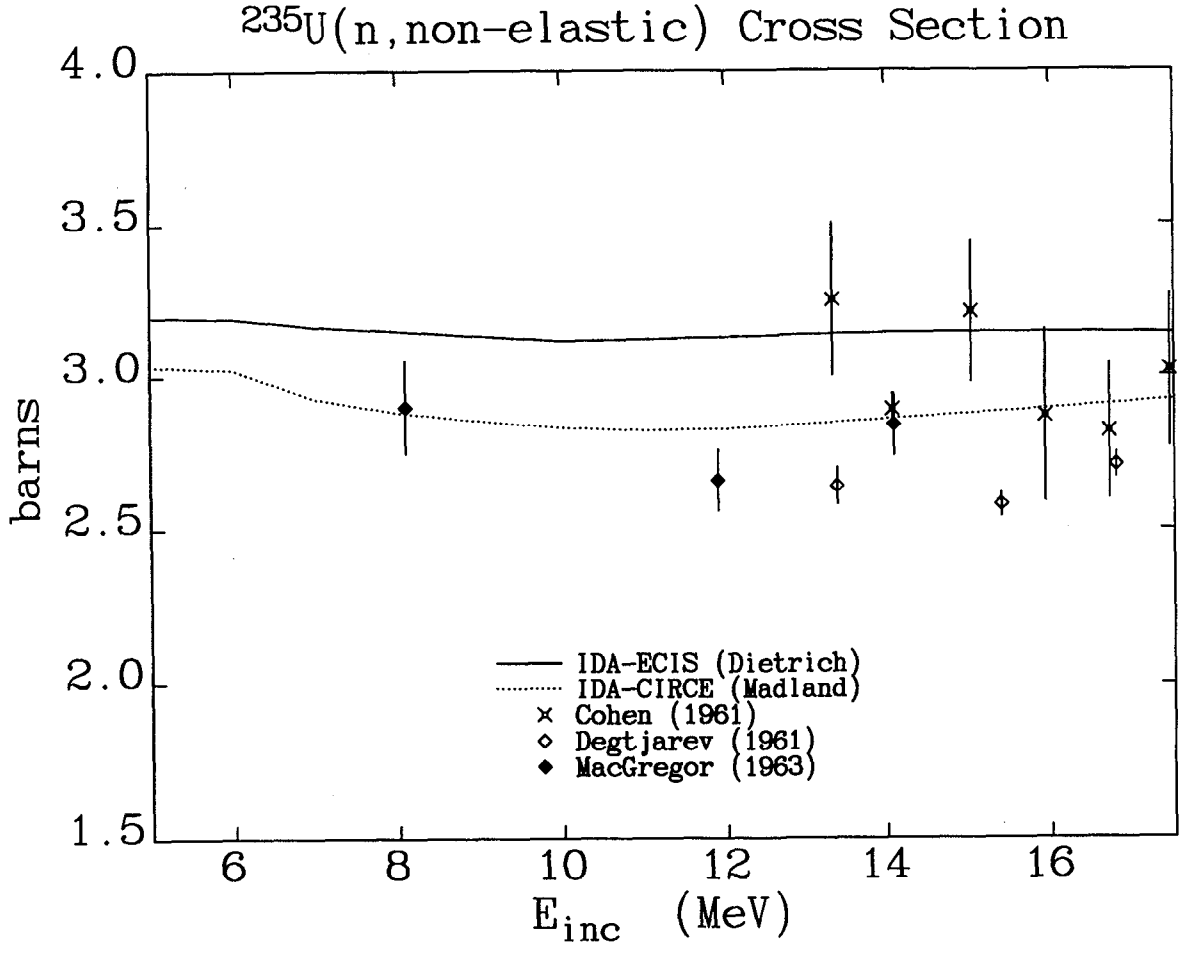

Figure 2: *Non-elastic cross section of the n+^{235}U reaction as a function of incident neutron energy.*

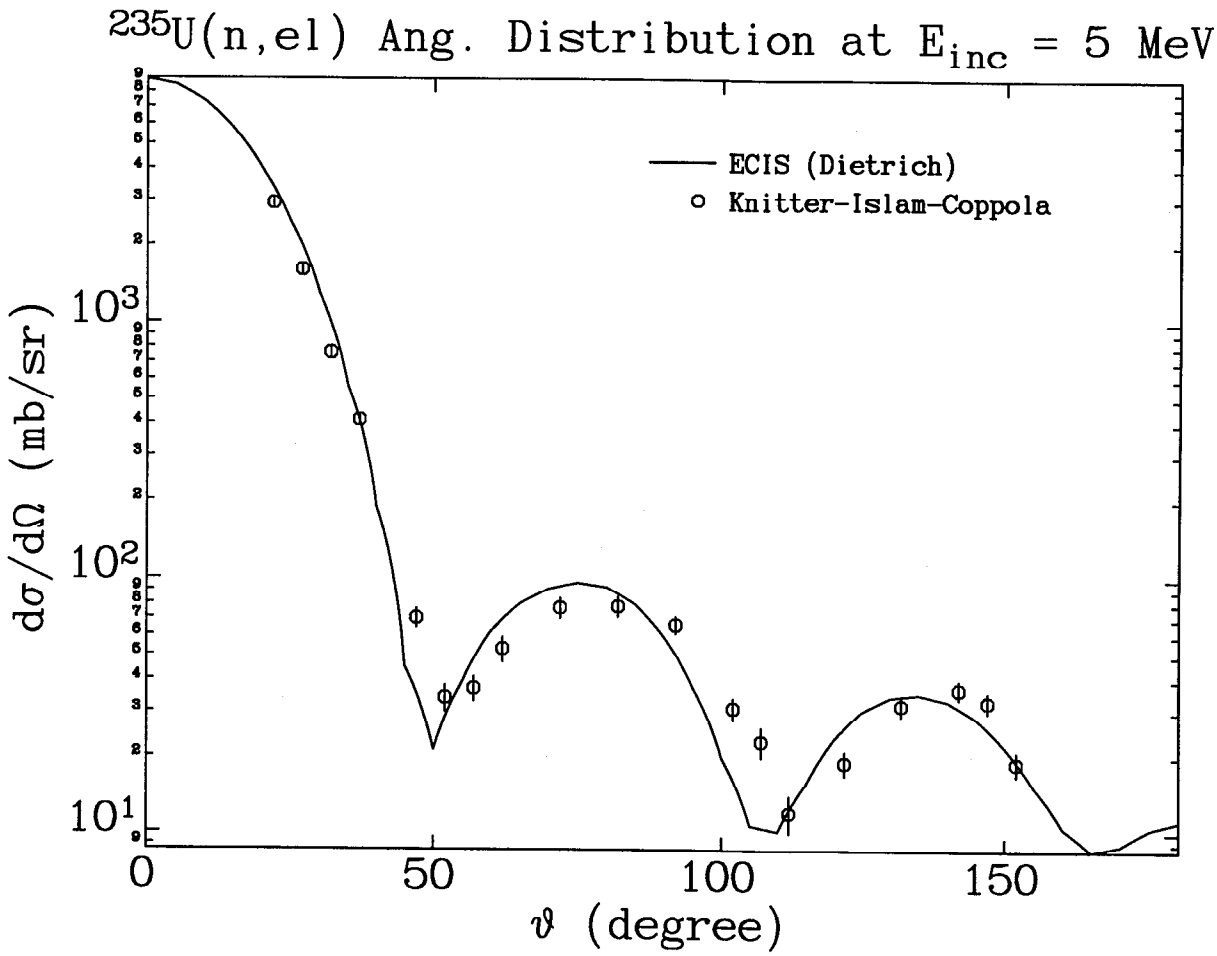

Figure 3: $^{235}U(n, \text{elastic})$ *angular distribution at* $E_{\text{inc}} = 5.0$ *MeV.*

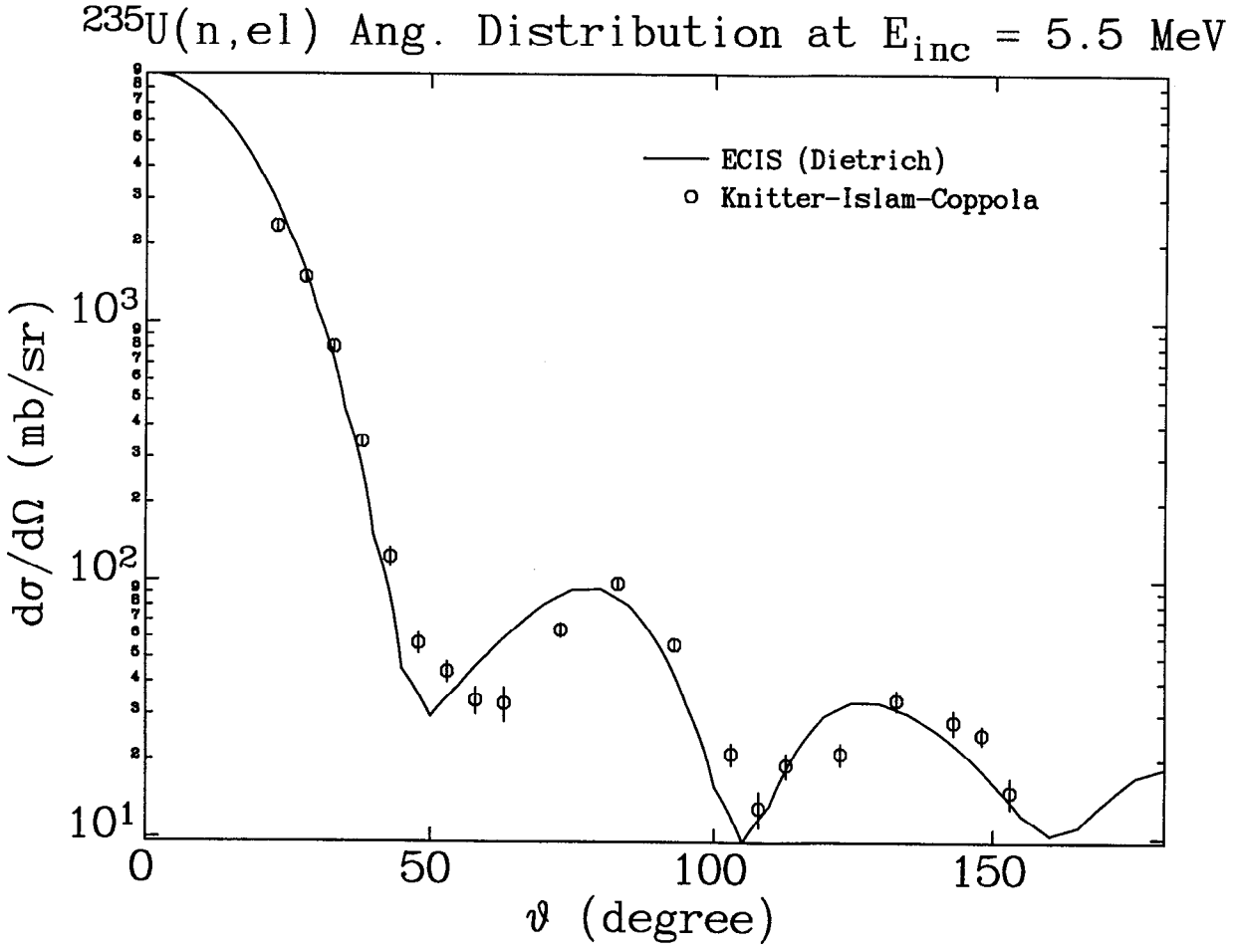

Figure 4: $^{235}U(n, \text{elastic})$ *angular distribution at* $E_{\text{inc}} = 5.5$ *MeV.*

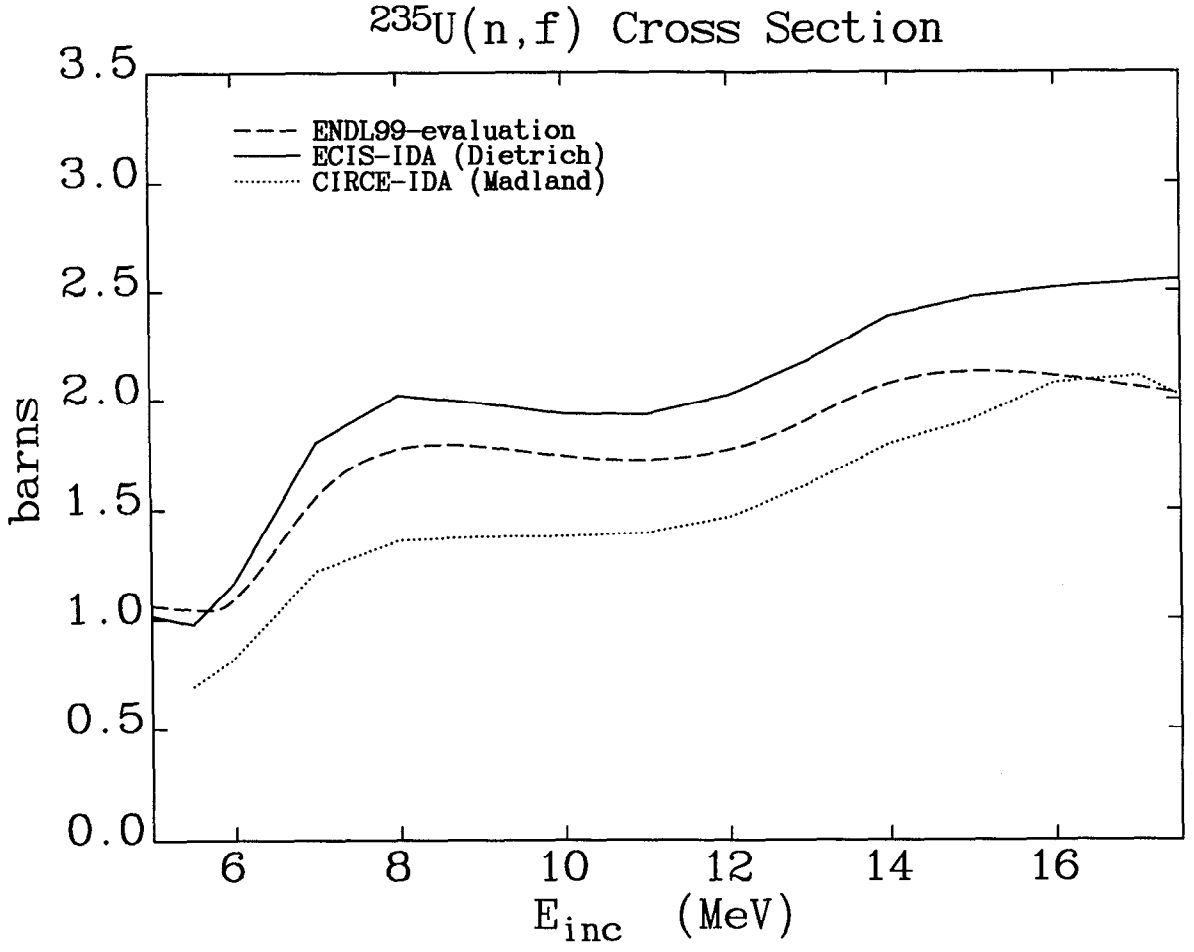

Figure 5: $^{235}U(n,f)$ *cross section as a function of incident neutron energy.*

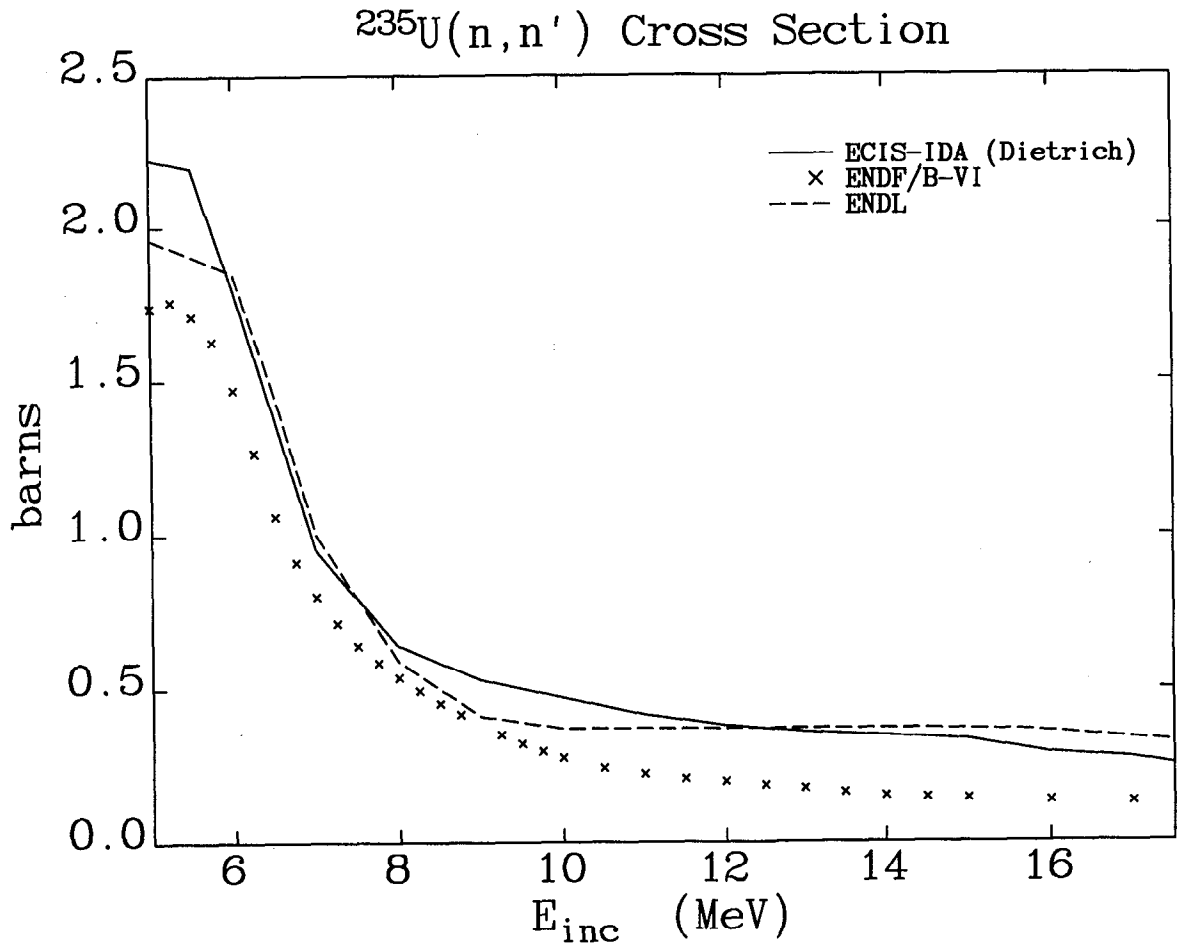

Figure 6: $^{235}U(n,n')$ *cross section as a function of incident neutron energy.*

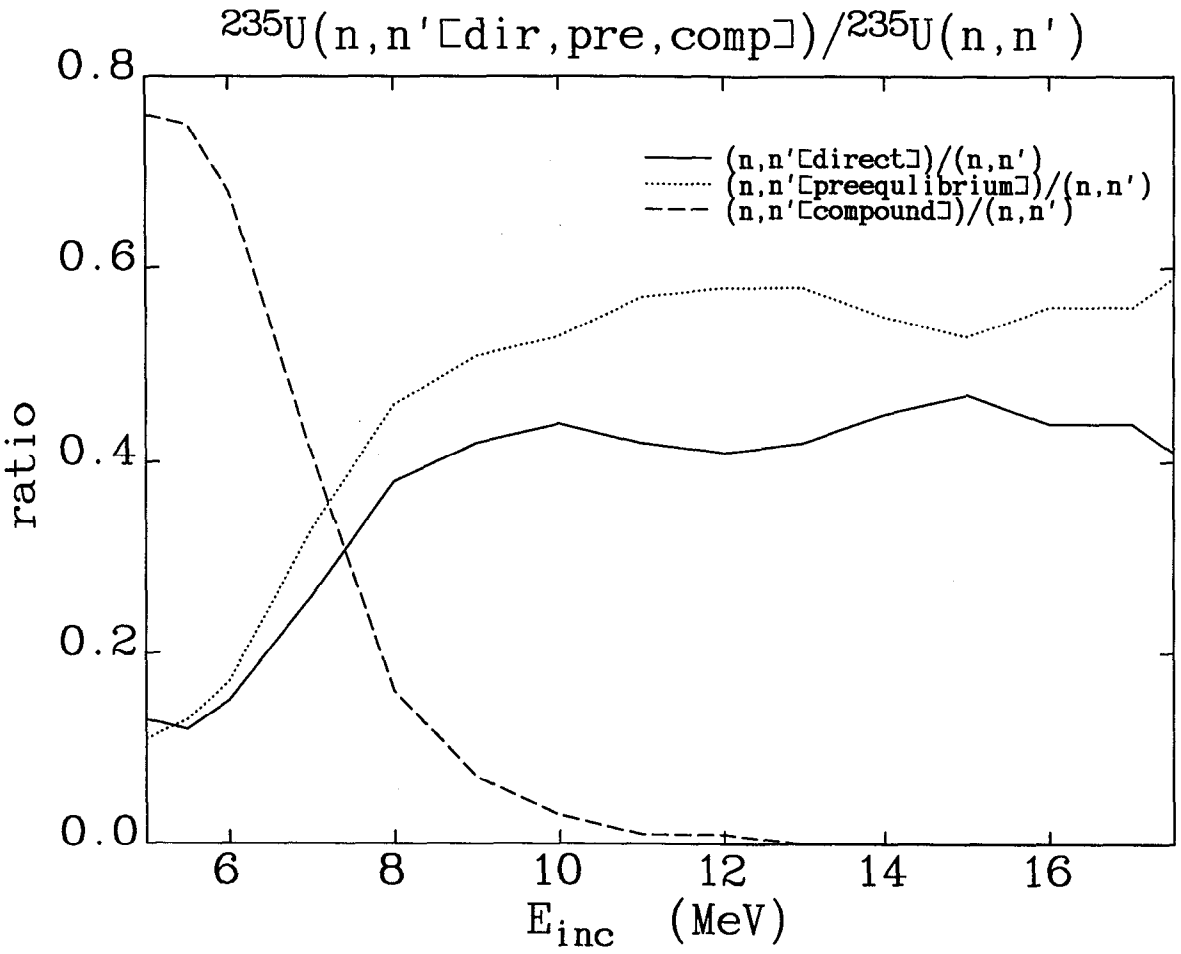

Figure 7: *Ratios of the direct, preequilibrium and compound components of* $^{235}U(n,n')$ *to the total* $^{235}U(n,n')$ *cross section as functions of incident neutron energy.*

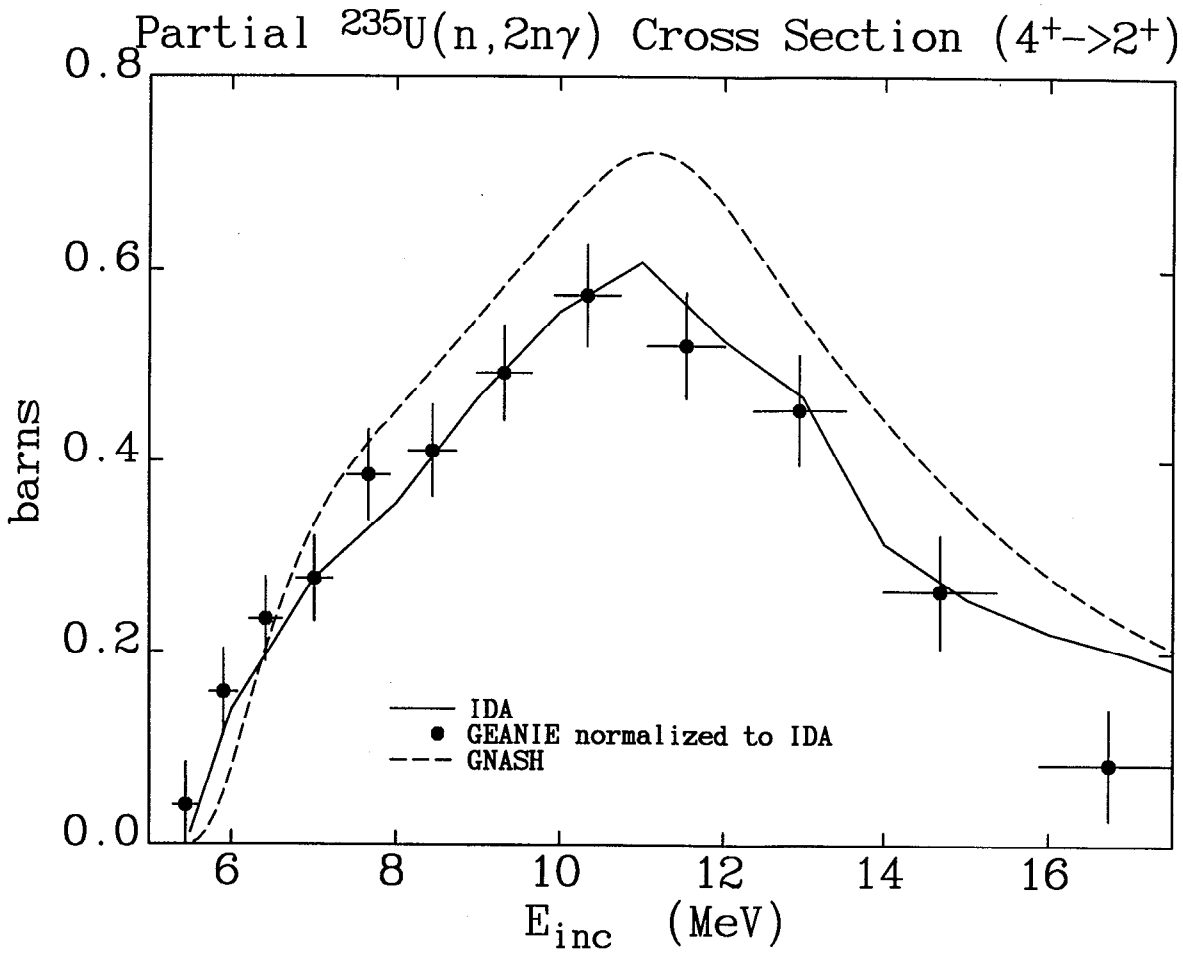

Figure 8: *Calculated and measured* $4_1^+ \rightarrow 2_1^+$ *excitation function for the* ^{234}U *nucleus.*

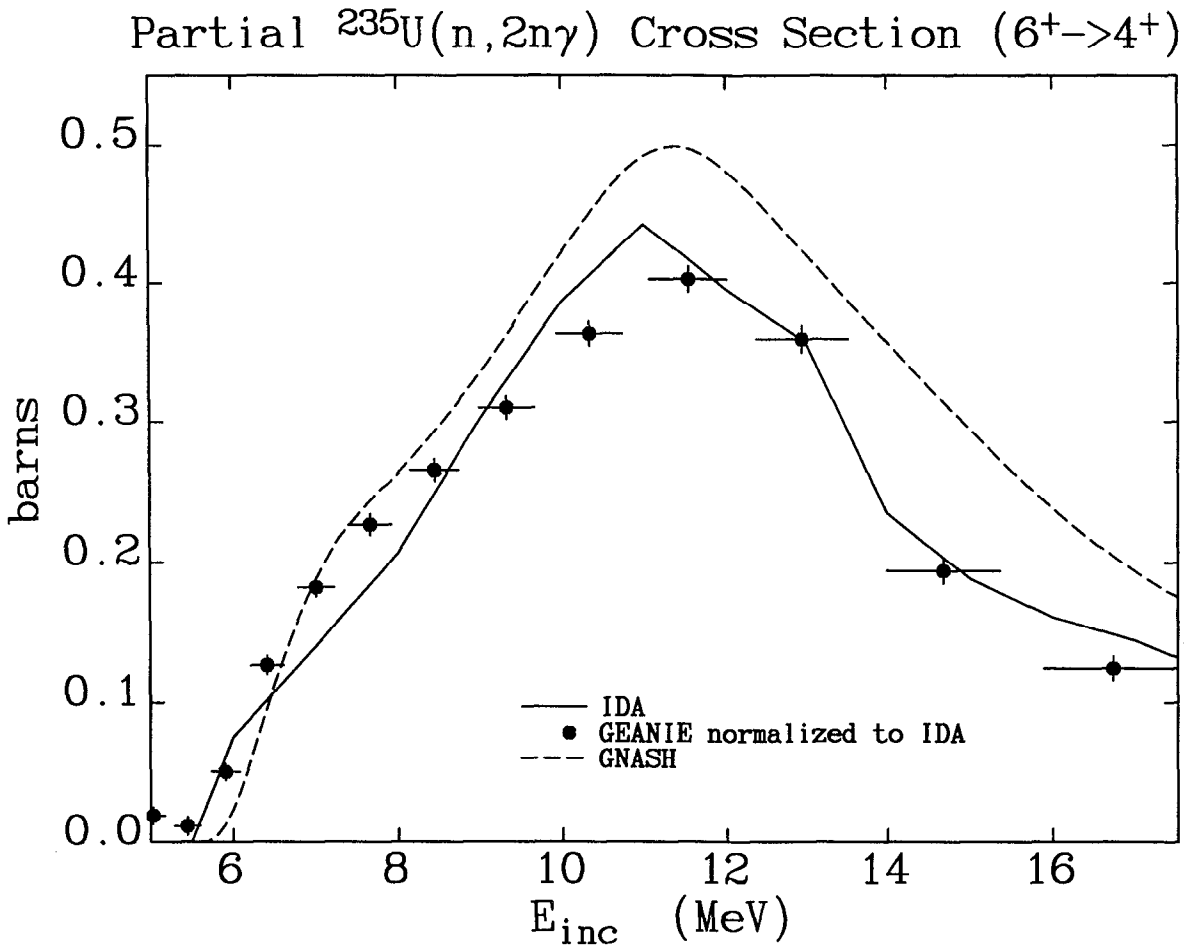

Figure 9: *Calculated and measured* $6_1^+ \rightarrow 4_1^+$ *excitation function for the* ^{234}U *nucleus.*

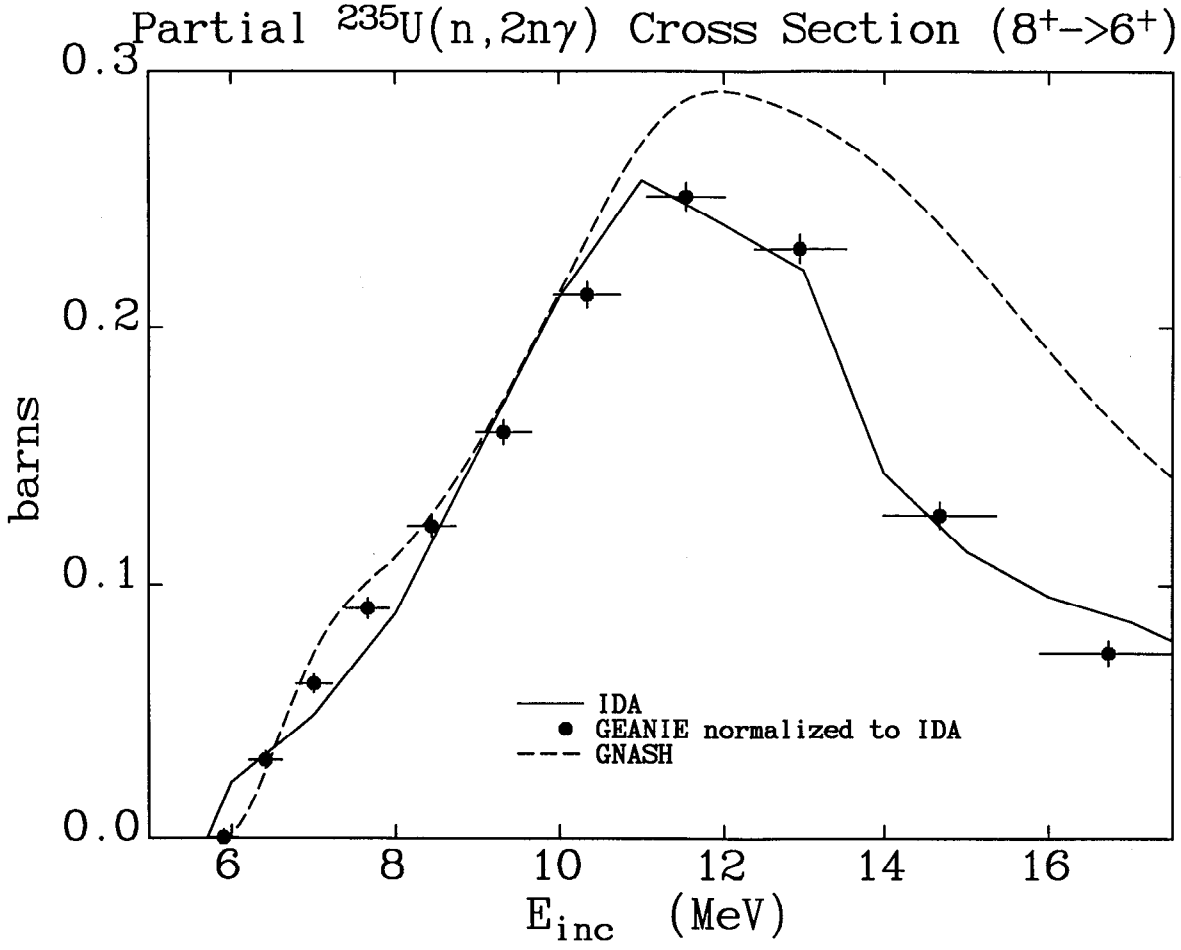

Figure 10: *Calculated and measured* $8_1^+ \rightarrow 6_1^+$ *excitation function for the* ^{234}U *nucleus.*

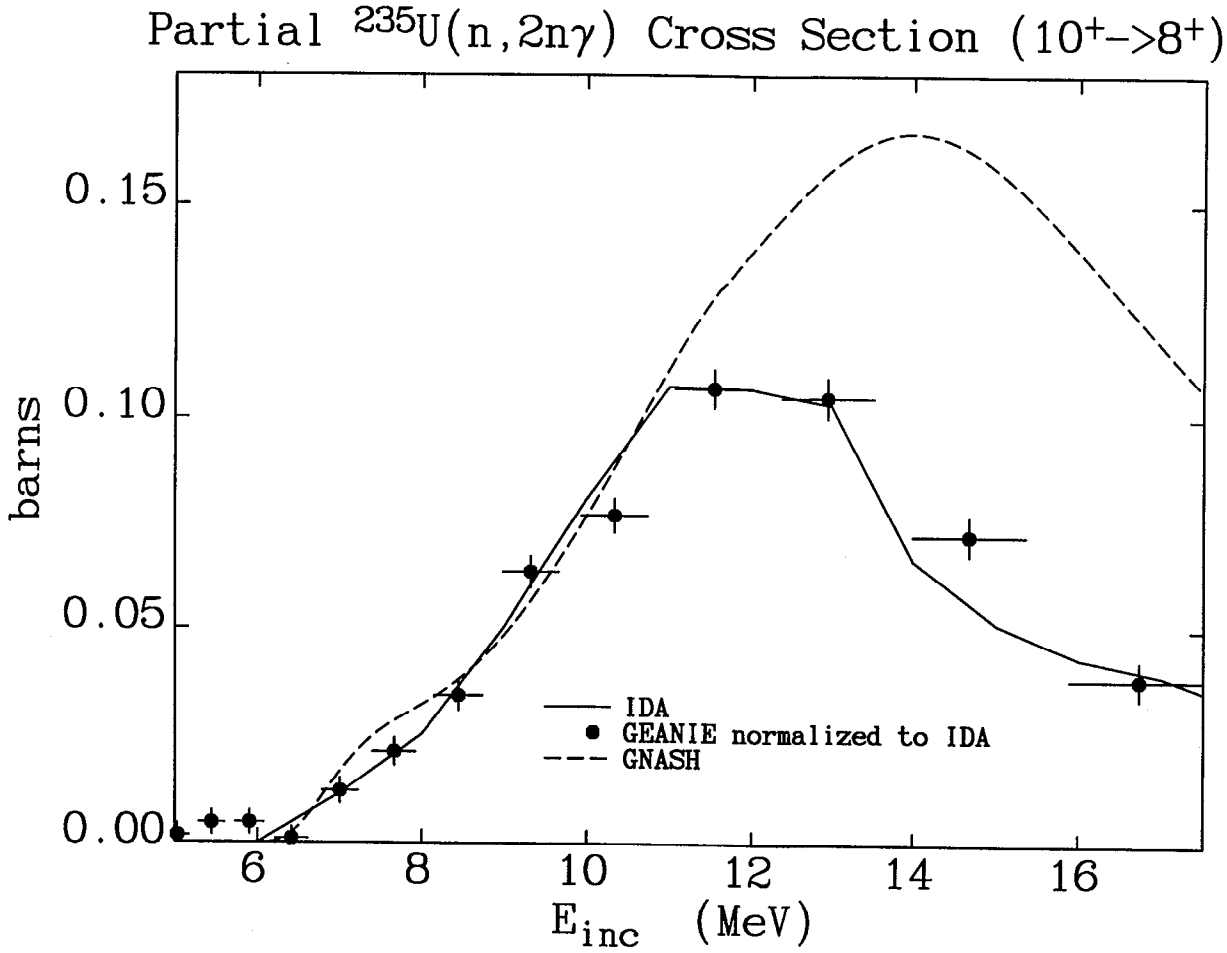

Figure 11: *Calculated and measured* $10_1^+ \rightarrow 8_1^+$ *excitation function for the* ^{234}U *nucleus.*

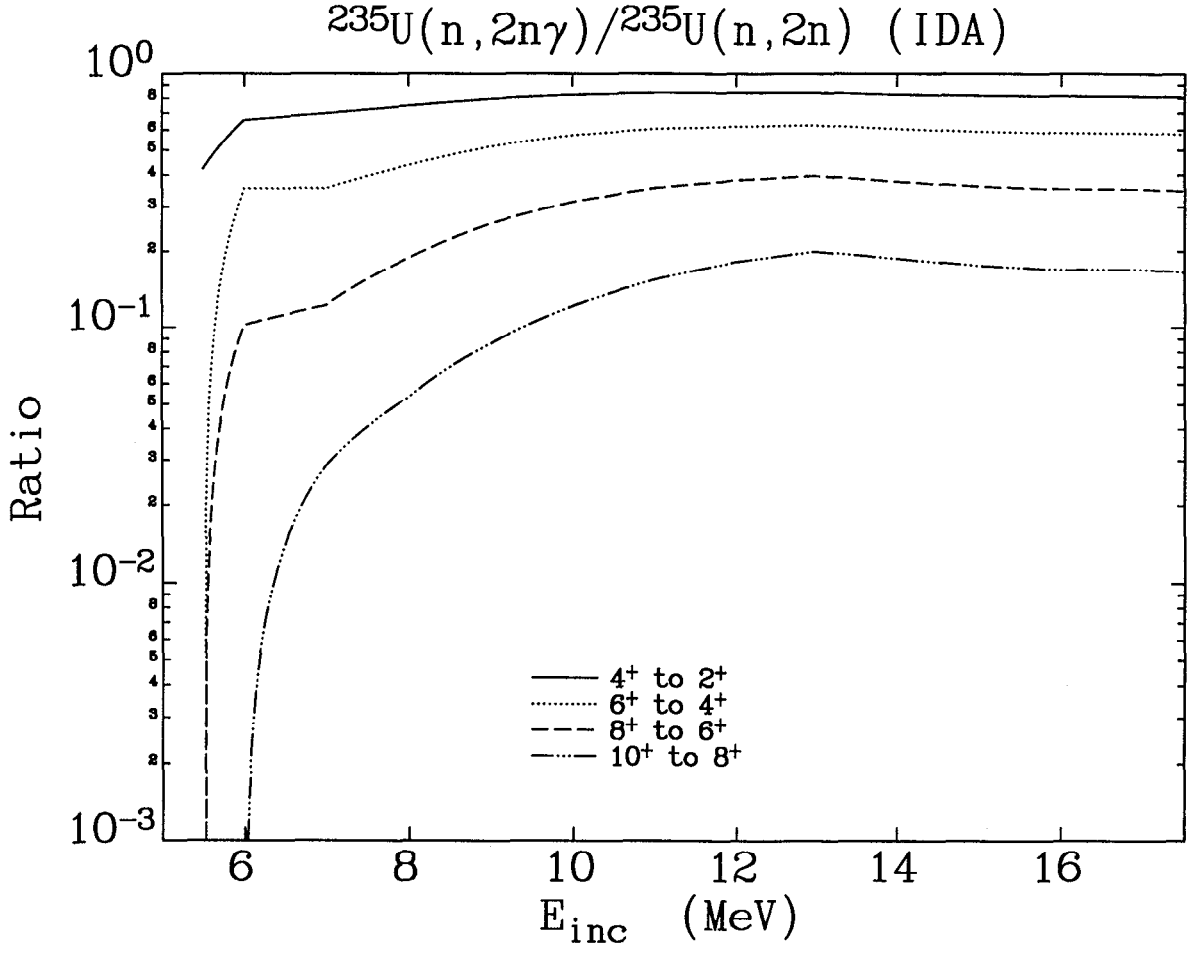

Figure 12: *Calculated ratios of* $^{235}\mathrm{U}(n,2n\gamma^{4_1^+\to 2_1^+})^{234}\mathrm{U}/^{235}\mathrm{U}(n,2n)^{234}\mathrm{U}$, $^{235}\mathrm{U}(n,2n\gamma^{6_1^+\to 4_1^+})^{234}\mathrm{U}/^{235}\mathrm{U}(n,2n)^{234}\mathrm{U}$, $^{235}\mathrm{U}(n,2n\gamma^{8_1^+\to 6_1^+})^{234}\mathrm{U}/^{235}\mathrm{U}(n,2n)^{234}\mathrm{U}$, $^{235}\mathrm{U}(n,2n\gamma^{10_1^+\to 8_1^+})^{234}\mathrm{U}/^{235}\mathrm{U}(n,2n)^{234}\mathrm{U}$ *as a function of incident neutron energy.*

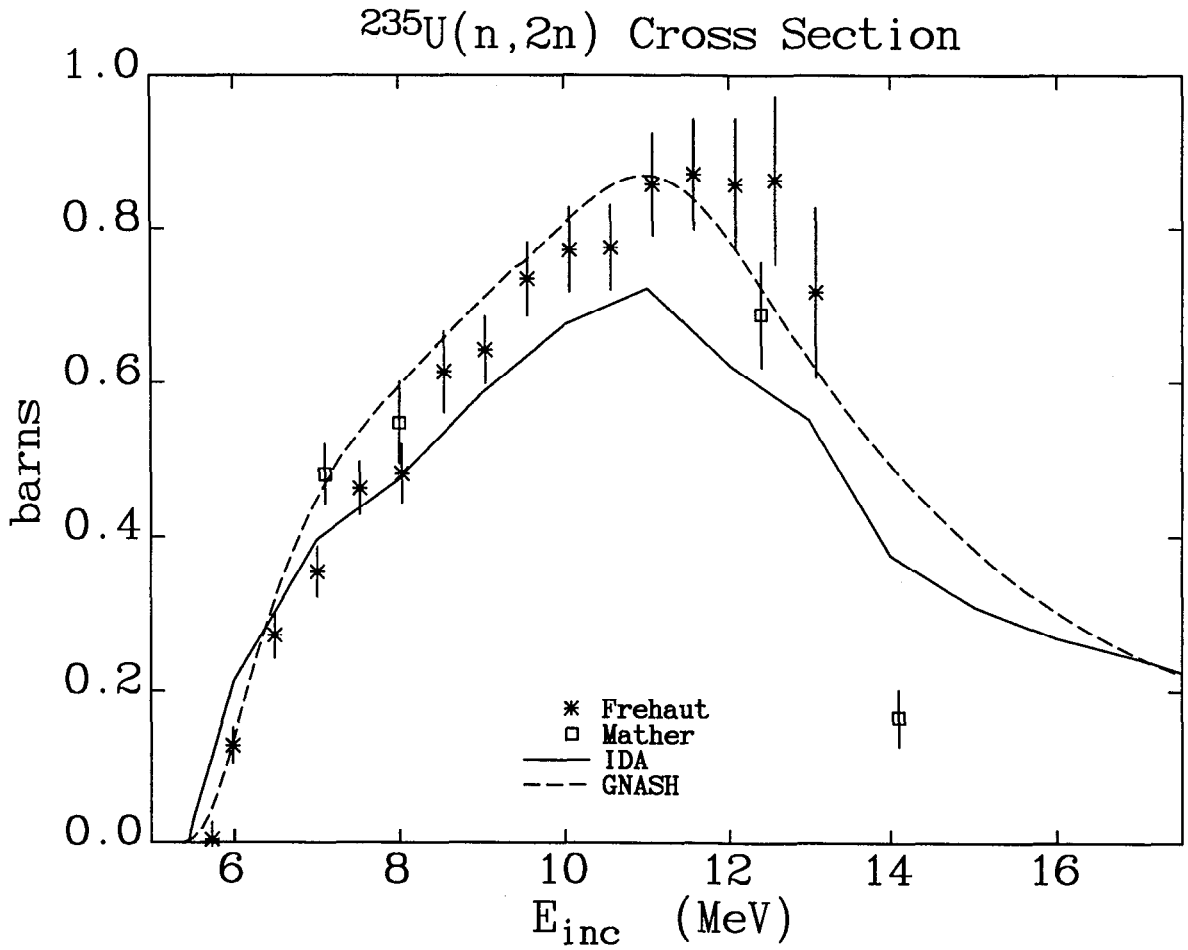

Figure 13: *Total* $^{235}\mathrm{U}(n,2n)^{234}\mathrm{U}$ *cross section, as a function of incident neutron energies, calculated by IDA and measured by Frehaut and Mather.*

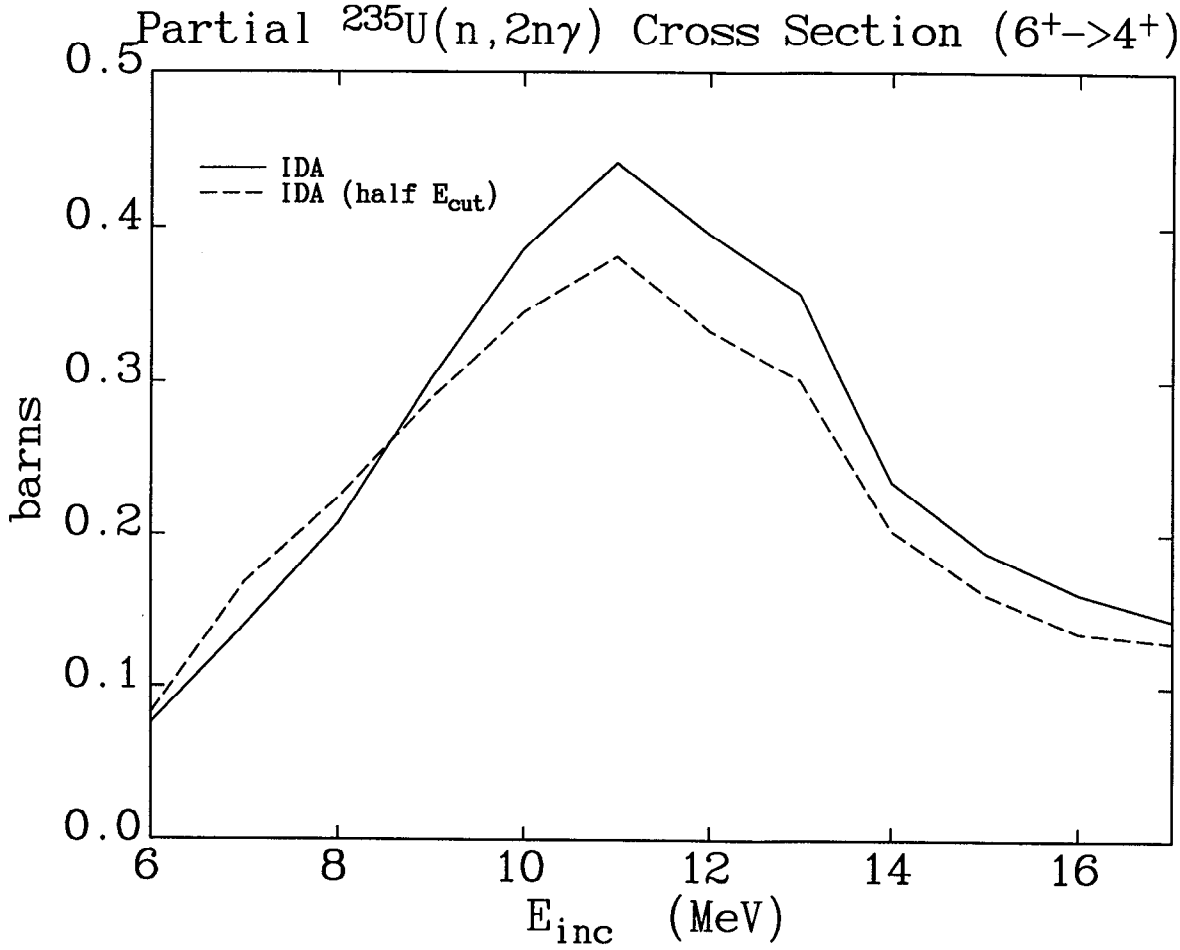

Figure 14: *Excitation functions of the* $6_1^+ \rightarrow 4_1^+$ *transition in the* ^{234}U *nucleus calculated at* $E_{\rm cut} = 1.14$ *MeV and at half this value (see text for discussion of* $E_{\rm cut}$*).*

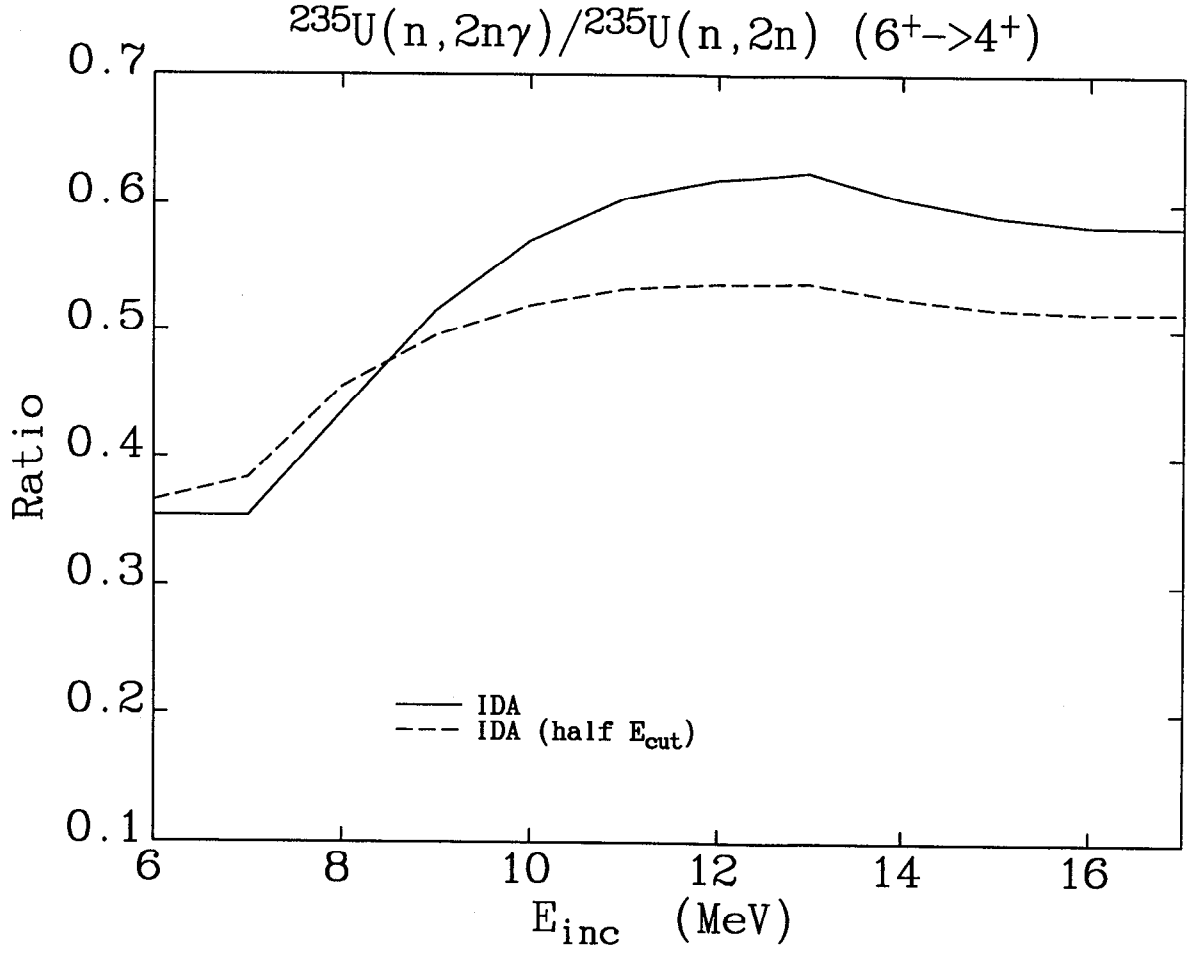

Figure 15: *The ratios of* $^{235}\mathrm{U}(n, 2n\gamma^{6_1^+ \to 4_1^+})/^{235}\mathrm{U}(n, 2n)$ *calculated at* $E_{\mathrm{cut}} = 1.14$ *MeV and at half this value.*

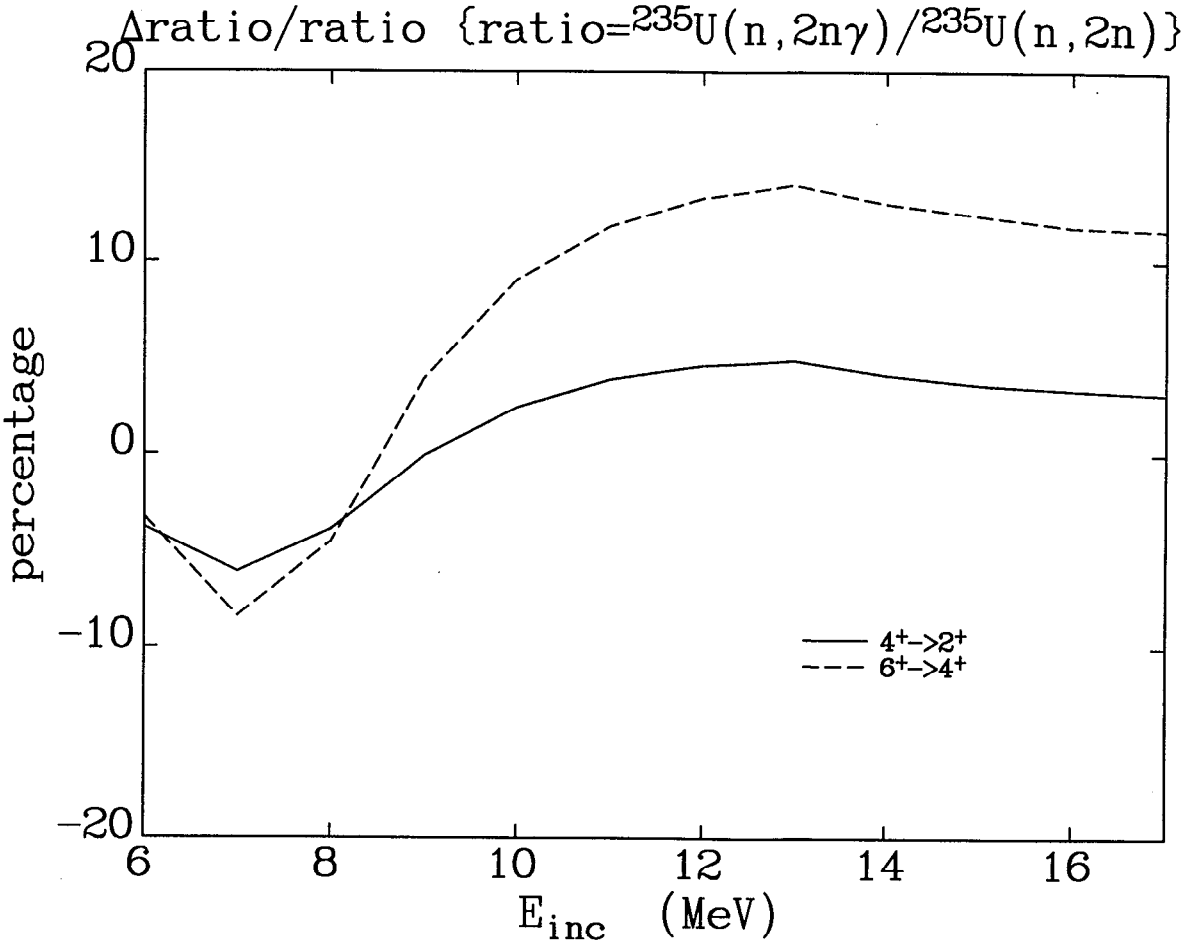

Figure 16: *The percentage change, due to the reduction of* $E_{\rm cut}$ *to half its original value, of the ratios* $^{235}{\rm U}(n,2n\gamma^{6_1^+\to 4_1^+})/^{235}{\rm U}(n,2n)$ *and* $^{235}{\rm U}(n,2n\gamma^{4_1^+\to 2_1^+})/^{235}{\rm U}(n,2n)$*, as a function of incident neutron energy.*